Available online at www.sciencedirect.com
ScienceDirect
Trans. Nonferrous Met. Soc. China 24(2014) 2179−2186
Transactions of Nonferrous Metals Society of China
www.tnmsc.cn

Dynamic mechanical properties and constitutive equations of 2519A aluminum alloy

Wen-hui LIU, Zhen-tao HE, Yu-qiang CHEN, Si-wen TANG

School of Electromechanical Engineering, Hunan University of Science and Technology, Xiangtan 411201, China

Received 17 October 2013; accepted 15 May 2014

Abstract: To analyze the effects of strain rate and temperature on the flow stress of 2519A aluminum alloy, the dynamic mechanical properties of 2519A aluminum alloy were measured by dynamic impact tests and quasi-static tensile tests. The effects of strain rate and temperature on the microstructure evolution were investigated by optical microscopy (OM) and transmission electron microscopy (TEM). The experimental results indicate that 2519A aluminum alloy exhibits strain-rate dependence and temperature susceptibility under dynamic impact. The constitutive constants for Johnson–Cook material model were determined by the quasi-static tests and Hopkinson bar experiments using the methods of variable separation and nonlinear fitting. The constitutive equation seems to be consistent with the experimental results, which provides reference for mechanical characteristics and numerical simulation of ballistic performance.

Key words: 2519A aluminum alloy; dynamic mechanical properties; Johnson-Cook model; microstructure

1 Introduction

2519A aluminum alloy, developed as one of the armor materials in the late 1980s, shows superior performance in contrast to other alternative aluminum alloys in terms of specific strength, good weldability and stress corrosion resistance [1]. Recently, the alloy has received a number of studies involving welding performance and microstructure evolution, but little research about the dynamic mechanical properties and constitutive equations has been done. ZHANG et al [2−6] used the thermal simulation setup and split Hopkinson pressure bar (SHPB) to study the quasi-static and dynamic property of 2519A aluminum alloy. They pointed out that the dislocation density had a association with strain rate during material strengthening process, and the θ' precipitate was affected by temperature significantly during material softening process. Meanwhile, the "single-factor" Cowper-Symonds and thermal activation Zener-Hollomon material models were employed to describe the plastic behavior of 2519A aluminum alloy. However, these two material models exhibited some limitations in terms of coupling of strain, temperature and strain rate, especially when they were applied to the numerical simulation of high-velocity impact. LIN et al [7] established BP artificial neural network with a single hidden layer to predict the hot deformation behavior of 2519A aluminum alloy. However, the accuracy of the material model tends to depend on the experiment data. Most importantly, this network model is rarely applied to numerical simulations. Furthermore, some researchers [8−10] focused on the microstructure evolution around the crater in high-velocity impact experiments. However, most of the above researchers did not completely describe the microstructure evolution of 2519A aluminum alloy at different temperatures. Also, there are no effective parameters of constitutive equation for numerical simulation of this alloy under high speed impact.

The Johnson-Cook model, proposed in 1983 [11], was extensively used to describe the dynamic response of materials under impact load. The present work is to investigate the dynamic mechanical properties involving microstructure evolution and acquire the Johnson-Cook model parameters of 2519A aluminum alloy based on the

Foundation item: Project (51105139) supported by the National Natural Science Foundation of China; Project (14JJ5015) supported by the Hunan Provincial Natural Science Foundation of China; Project (HPCM-2013-03) supported by the Open Research Fund of Key Laboratory of High Performance Complex Manufacturing, Central South University, China

Corresponding author: Wen-hui LIU; Tel: +86-18873216868; E-mail: lwh@hnust.edu.cn

DOI: 10.1016/S1003-6326(14)63330-6

quasi-static tensile tests and dynamic impact tests, which provide a useful reference for numerical simulation of ballistic performance.

2 Experimental

The plate specimens prepared for quasi-static tensile tests and cylindrical specimens prepared for dynamic compression tests were taken from an identical 18 mm thick sheet of 2519A-T87 aluminum alloy. The tensile direction was parallel to the rolling direction, and the impact direction was parallel to the plate normal direction. The quasi-static tests were conducted by the electronic universal testing machine at strain rates of 0.001, 0.01 and 0.1 s^{-1}, respectively. The quasi-static test result at strain rate of 0.01 s^{-1} was selected as the reference to determine the strain hardening parameters of constitutive equation. The dynamic impact tests at room temperature (20 °C) were performed by the SHPB system under nominal strain rates of 1500, 2400, 3000, 4300, 5600, 7000 and 8300 s^{-1}. The dynamic impact tests at the temperatures of 150, 250 and 350 °C were performed at strain rates of 1000−5000 s^{-1}. Samples selected for metallographic microstructure characterization were polished and etched with Keller's reagent composed of 95 mL H_2O, 2.5 mL HNO_3, 1.5 mL HCl and 1.0 mL HF. Samples selected for electron microstructure characterization were mechanical polished to 0.1 mm thickness and electropolished in an acid solution containing 30 mL nitric acid and 70 mL methyl alcohol cooled to about −25 °C at a voltage of 15−20 V, and then were examined by a Tecnai $G^2$20 analytical transmission electron microscope.

3 Results and discussion

3.1 Stress−strain behavior

The stress−strain relations at room temperature under the strain rate of 0.001−8300 s^{-1} are shown in Fig. 1(a). The stress−strain curves at 150 °C to 350 °C are shown in Figs. 1(b)−(d). Compared to the quasi-static case, the flow stresses of dynamic impact have a little instability near the yield point, then they become steady after plastic deformation, which indicates that the force equilibrium is obtained only after plastic deformation [12]. The higher the strain rate is, the more obvious the fluctuations of the flow stress near the yield point are. The strain rate strengthening effect is obvious at 20 and 150 °C, especially when strain rate exceeds 3300 s^{-1}. At room temperature, the flow stress drops a little when the strain rate exceeds 6962.25 s^{-1}, which indicates that there is a peak value of strain rate to strengthen the

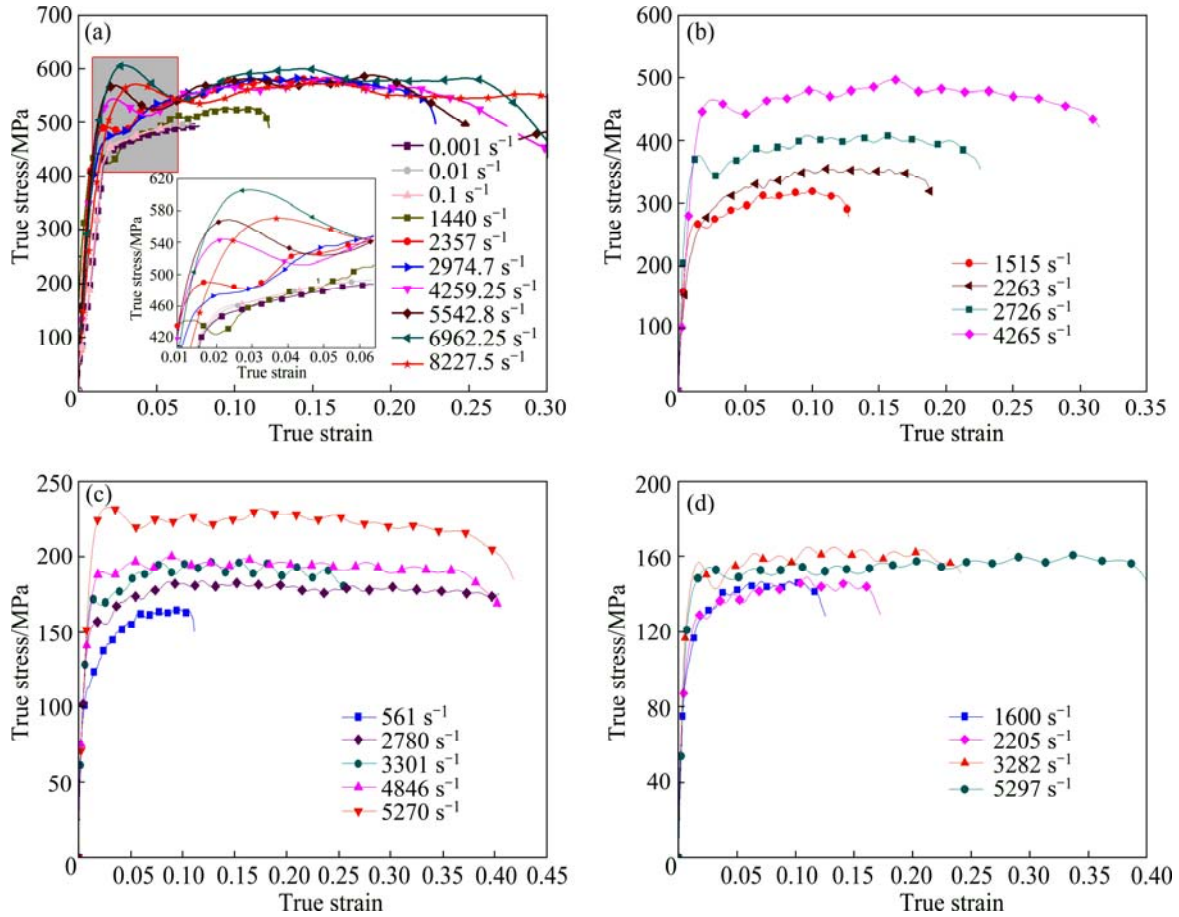

Fig. 1 Stress−strain curves of different strain rates at different temperatures: (a) 20 °C; (b) 150 °C; (c) 250 °C; (d) 350 °C

material [4]. In the elevated testing temperature region, the flow curves present a wavy response due to the dynamic recrystallization in adiabatic shear bands (ASBs) [5].

From Figs. 2 and 3, it can be seen that 2519A aluminum alloy exhibits strain rate sensitivity and strong temperature susceptibility. At room temperature, the yield stress increases with strain rate increasing, but decreases a little when the strain rate reaches 8227.5 s^{-1}. When the testing temperature is 150 °C, the yield stress increases rapidly especially under strain rate of 3000−5000 s^{-1}, while it increases slowly when the testing temperature is 250−350 °C. Namely, the strengthening effect of strain rate is obvious at normal temperature (20−150 °C), and the reason may be the interaction of high density dislocation and θ' precipitate pinning effect [4]. However, this effect is not obvious for temperature exceeding 250 °C, and the reason can be referred to the shape change of θ' precipitate [4]. In Fig. 3, it can be found that the yield stress decreases sharply with the temperature increasing, especially for the temperature from 150 °C to 250 °C, which indicates that the temperature is the key role in material softening process.

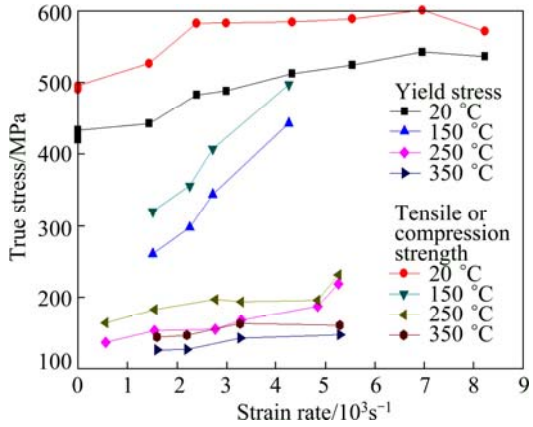

Fig. 2 Effect of strain rate on yield stress and tensile/compression strength

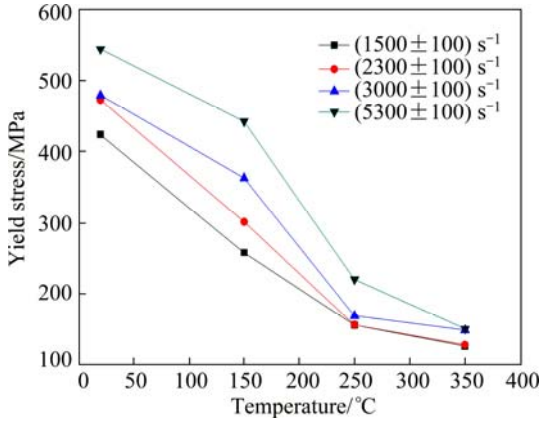

Fig. 3 Effect of temperature on yield stress at different strain rates

3.2 Constitutive analysis

The material's constitutive equation is the key factor in the finite element method simulations. There are some viscoplasticity strength models to describe the behavior of viscoplasticity, such as Cowper-Symonds, Zener-Hollomon and Zerilli-Armstrong models. The Johnson-Cook model, considering the effects of strain, strain rate and deformation temperature, is widely used in the high strain rate situation of molding, cutting, crash, perforation and so on. The model, expressing the relation of von Mises flow stress and strain, is shown as follows:

$$\sigma=(A+B\varepsilon^{n})(1+C\ln\dot{\varepsilon}^{*})(1-T^{*m}) \quad (1)$$

where σ is the von Mises flow stress; ε is the equivalent plastic strain; $\dot{\varepsilon}^{*}=\dot{\varepsilon}/\dot{\varepsilon}_0$ represents the dimensionless plastic strain rate ($\dot{\varepsilon}$ is the strain rate, $\dot{\varepsilon}_0$ is the reference strain rate); $T^{*}=(T-T_r)/(T_m-T_r)$ is the homologous temperature, T is the current temperature, T_r is the reference temperature, and T_m is the melting temperature. The five material parameters A, B, C, n, m represent the yield stress at the reference temperature, strain hardening modulus, coefficient of strain rate hardening, strain hardening exponent and thermal softening exponent, respectively. In this work, $\dot{\varepsilon}_0$=0.01 s^{-1}, T_r=20 °C, T_m=542 °C [13].

The coefficients and exponents of this model are determined by quasi-static tensile tests and SHPB tests. Considering the yield point of quasi-static tensile curves is not well defined, and also the yield stress value of the SHPB tests may be inaccurate [14,15], the methods of variable separation and nonlinear fitting in the software Origin are used. The five parameters of Johnson-Cook model A, B, C, n and m are calculated from the quasi-static and SHPB experimental data listed in Table 1. Comparisons between the experimental results and Johnson-Cook constitutive equation are shown in Fig. 4(a) and (b). It is shown that the Johnson-Cook constitutive equation is in agreement with the experimental data approximately. There is a critical point ($d\sigma/d\varepsilon$=0) in each dynamic impact curves. The 2519A aluminum alloy material undergoes a stable plastic deformation stage ($d\sigma/d\varepsilon$>0) in the region from the yield point to the critical point, and it undergoes an unstable plastic deformation stage ($d\sigma/d\varepsilon$<0) in the region after the critical point [16].

Table 1 Five parameters of Johuson-Cook constitutive equation with reference strain rate of 0.01 s^{-1} and 1 s^{-1}

$\dot{\varepsilon}_0$/s^{-1}	A/MPa	B/MPa	C	n	m
0.01	424.30	264.88	0.015197	0.42	0.74
1	452.68	282.60	0.014200	0.42	0.74

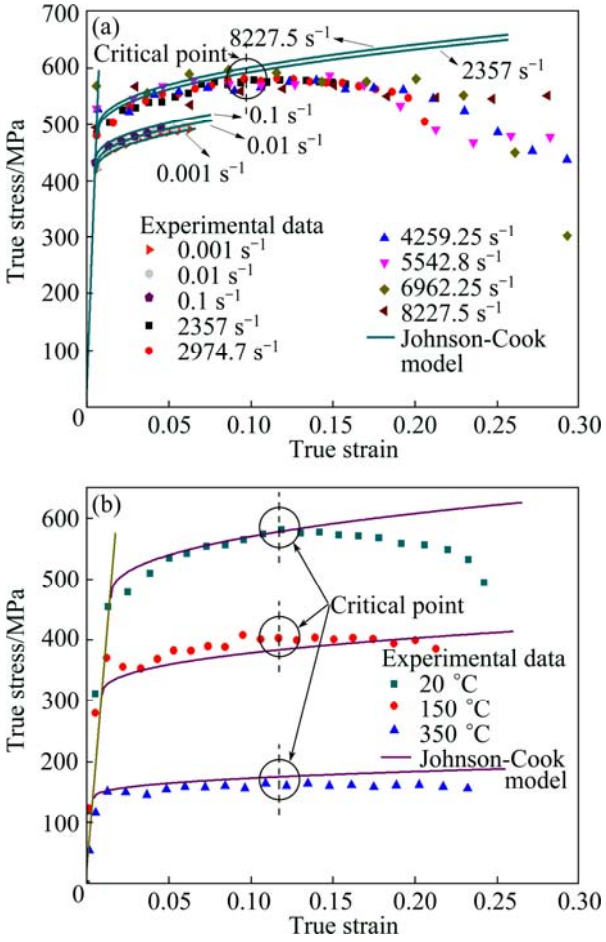

Fig. 4 Comparisons between experimental results and Johnson-Cook constitutive equation under different conditions: (a) Room temperature; (b) Elevated temperature ($\dot{\varepsilon}$=(3000±100) s^{-1})

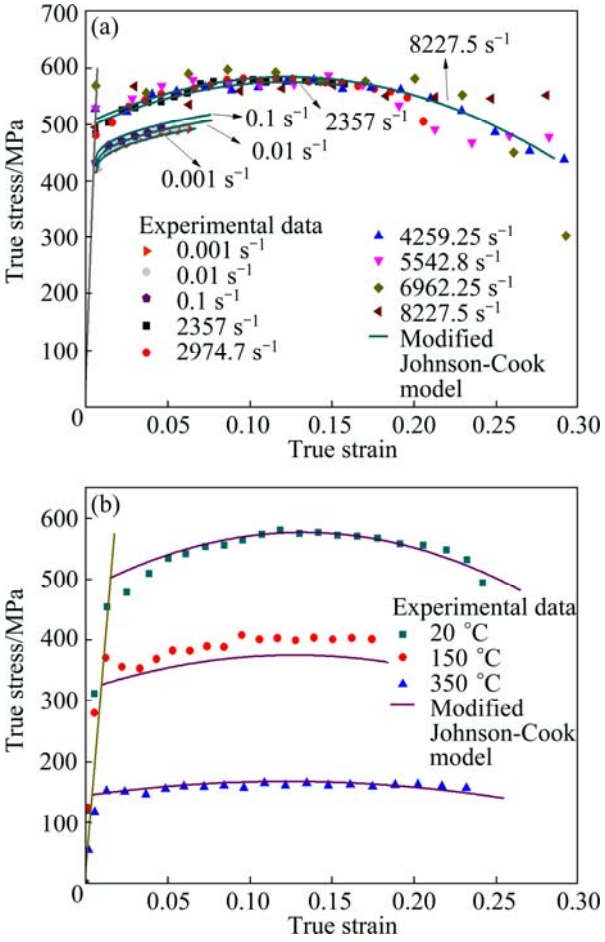

Fig. 5 Comparisons between experimental results and modified Johnson-Cook constitutive equation under different conditions: (a) Room temperature; (b) Elevated temperature ($\dot{\varepsilon}$=(3000±100) s^{-1})

The decrease of flow stress has a close relationship with the adiabatic shearing. When the effect of strain hardening exceeds that of thermal softening, the flow stress keeps a rising trend. When the effect of thermal softening exceeds that of strain hardening, the flow stress drops gradually. Therefore, there is a critical point in each dynamic true stress−strain curves. One quadratic interpolation is proposed for the modified Johnson-Cook constitutive equation, as follows:

$$\sigma = A(1+E\varepsilon+F\varepsilon^2)(1+C\ln\dot{\varepsilon}^*)(1-T^{*m}) \quad (2)$$

The quadratic interpolation shows a lower strain hardening than that from the Ludwik-Hollomon model [17]. The parameters E and F calculated by nonlinear fitting method are 2.54 and −10.8, respectively. The comparisons between experimental results and modified Johnson-Cook constitutive equation at room temperature and elevated temperature are shown in Fig. 5, and it can be found that the results of modified JC constitutive equation agree with experimental data better.

3.3 Microstructural observations

Adiabatic shearing is the main damage and fracture mechanism of 2519A aluminum alloy at high strain rate [2]. Figure 6(a) shows the ASB and crack which go through part of impacted specimen. It can be observed that a crack originated from the contact surface extends along the ASB. The material near the crack deforms largely (see Fig. 6(b)). An island shape block forms as a result of the intersection of two cracks. If the crack extends across the whole specimen, the specimen is separated into two pieces, and a plane of shearing is formed (see Fig. 6(c)).

The optical micrographs of 2519A aluminum alloy impacted at room temperature are shown in Fig. 7. The ASB and crack do not appear until strain rate reaches 2974.7 s^{-1}. The crack almost accompanies the ASB and branches extending to the free surface at strain rate of 5542.8 s^{-1}, so the island shape block is formed (see Figs. 7 (d) and (f)). Furthermore, the ASB and crack can be seen more obvious when the strain rate reaches

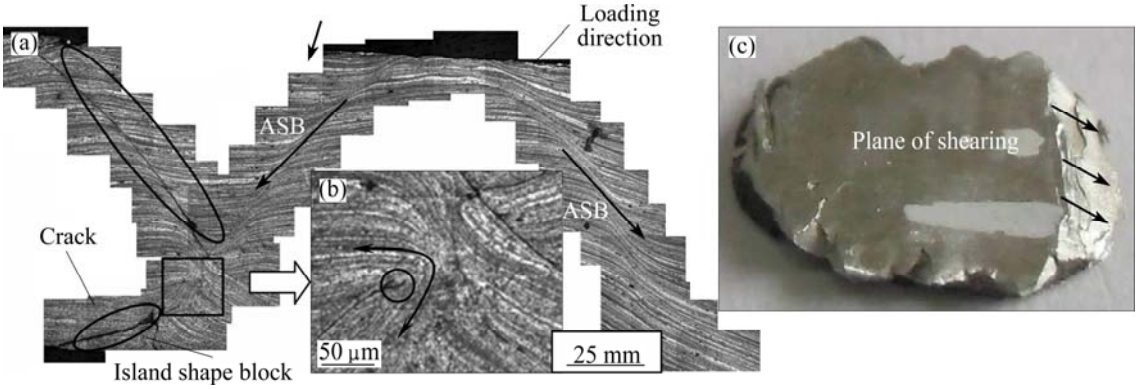

Fig. 6 Optical micrographs (a, b) and macroscopic fractography (c) of 2519A aluminum alloy impacted at strain rate of 6962.25 s^{-1} (20 °C)

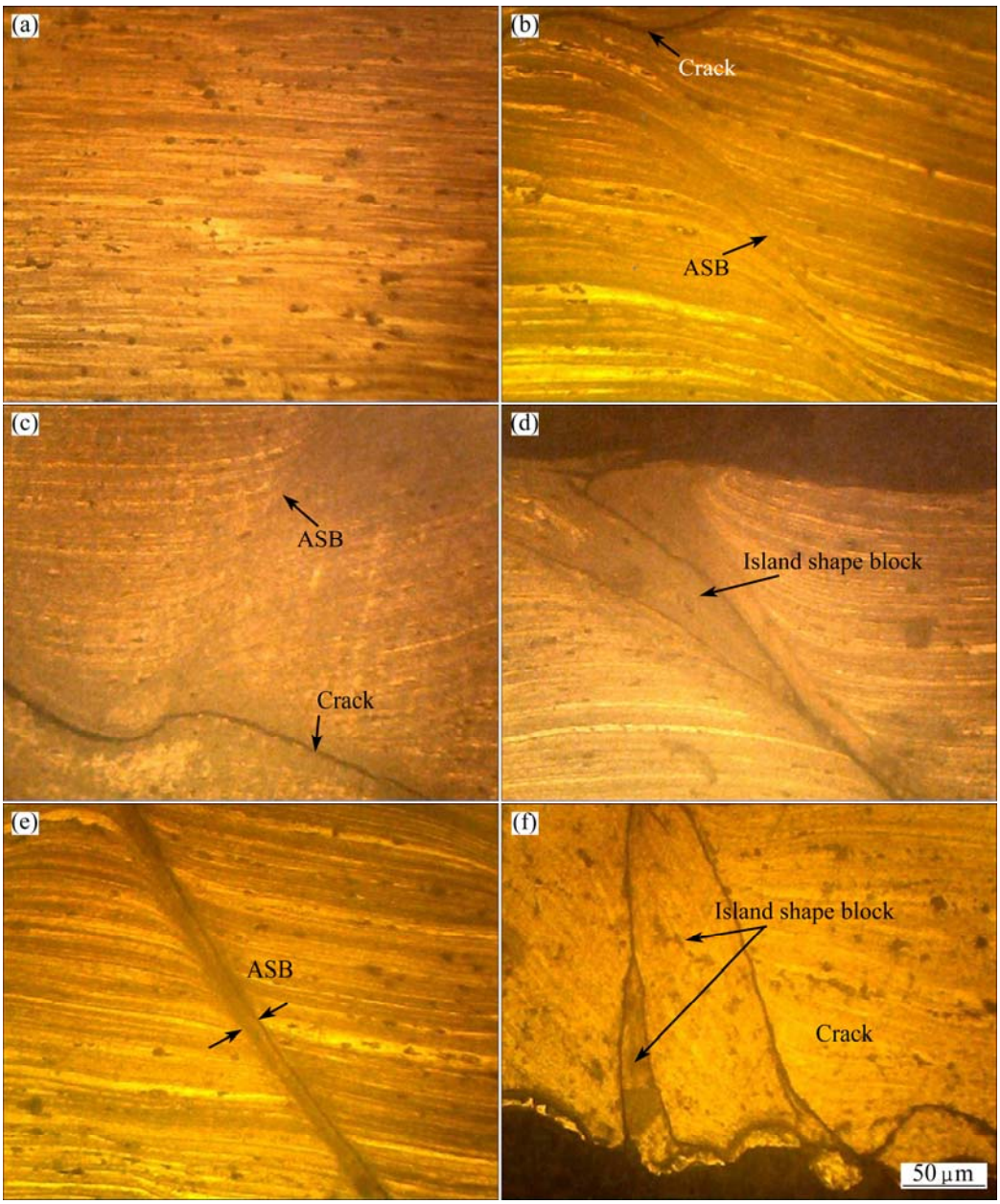

Fig. 7 Optical micrographs of 2519A aluminum alloy impacted at different strain rates: (a) 2357 s^{-1}; (b) 2974.7 s^{-1}; (c) 4259.25 s^{-1}; (d) 5542.8 s^{-1}; (e) 6962.25 s^{-1}; (f) 8227.5 s^{-1}

6962.25 s^{-1} (see Figs. 7(e) and (f)).

To investigate the microstructure evolution of 2519A aluminum alloy under dynamic impact at elevated temperature, the impacted specimen was cut from the cylindrical axis using wire-electrode cutting, as shown in Figs. 8(a) and (b). A number of deformation structures appear at the corner of the cylinder section of impacted specimen (see Fig. 8(c)). Some deformation structures distort severely and present spiral appearance, and there is no ASB in the impacted specimen. The above facts seem to indicate that 2519A aluminum alloy mainly undergoes large sliding and plastic deformation under dynamic impact at elevated temperature, and a quantity of impact energy is consumed in the way of sliding.

The features of metallography of 2519A aluminum alloy impacted at 150 °C and 350 °C are shown in Figs. 9 and 10. It can be found that the microstructure evolution impacted at 150 °C is similar to that impacted at room temperature, while it is inconsistent with that impacted at 350 °C. The end region of crack mainly presents the characteristic image of ASB (see Fig. 9(c)). The 2519A aluminum alloy material deforms in the way of sliding when temperature exceeds 150 °C.

In order to investigate the effect of temperature on the dynamic mechanical properties of 2519A aluminum alloy, the characteristic microstructures formed at elevated temperature and high strain rate are studied. The Al matrix and strengthening phase particles

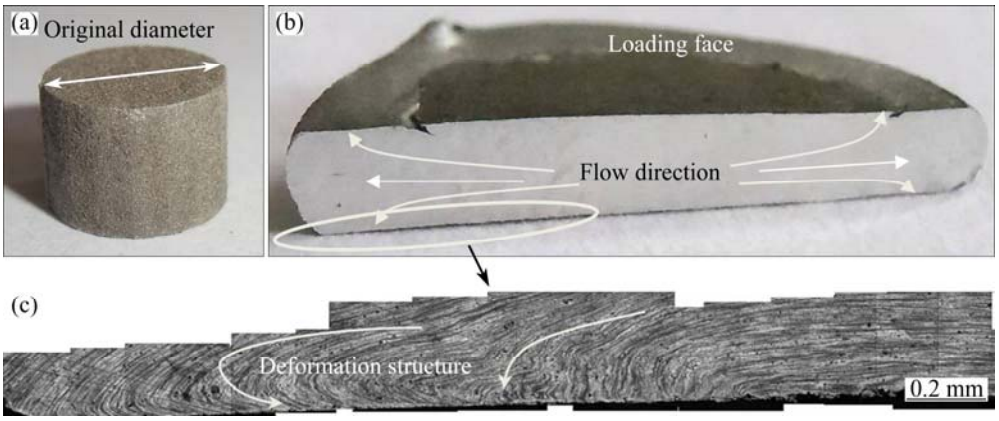

Fig. 8 Optical micrographs of 2519A aluminum alloy impacted at strain rate of 3282 s^{-1} (350 °C): (a) Sample before impact; (b) Sample after impact; (c) Deformation structure

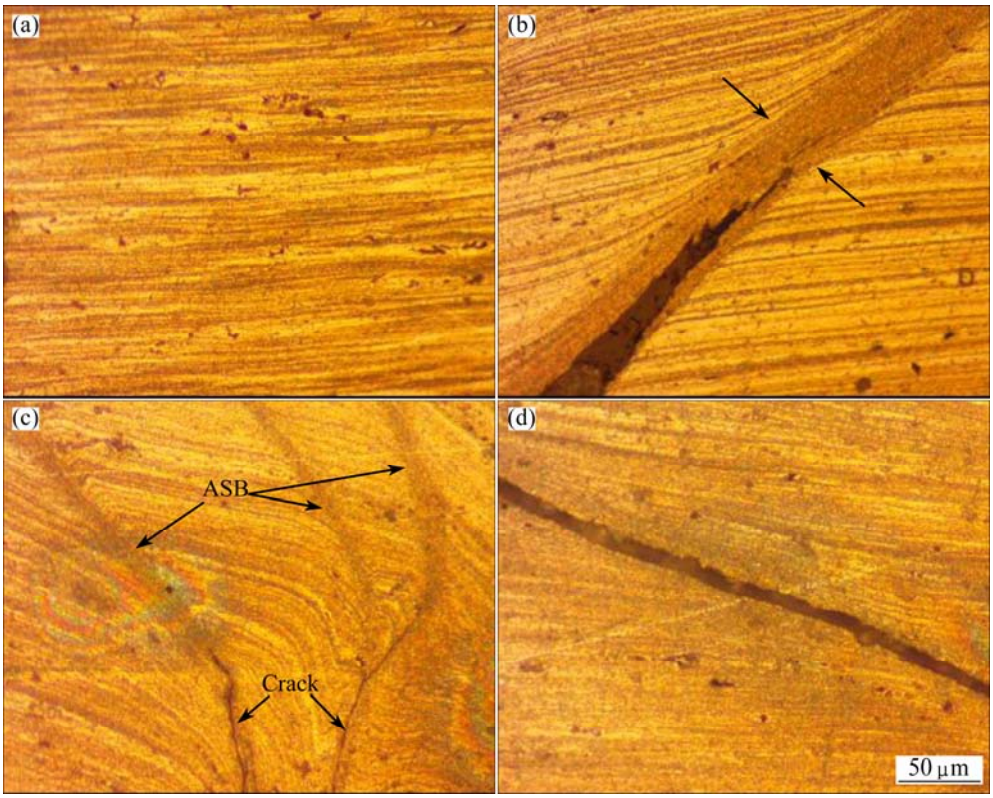

Fig. 9 Optical micrographs of 2519A aluminum alloy impacted at different strain rates (150 °C): (a) 1515 s^{-1}; (b) 2263 s^{-1}; (c) 2726 s^{-1}; (d) 4265 s^{-1}

keep coherency before dynamic impact loading (see Figs. 11(a) and (b)). The θ' precipitates thicken and coarsen when the specimen is hold for 5 min at 350 °C, as shown in Fig. 11(b). The precipitates thicken, coarsen and mostly present the spherical appearance after being impacted at elevated temperature and high strain rate after impacted. However, the interface between Al matrix and strengthening phase particles gradually transforms incoherency, and the number of θ' precipitate is greatly reduced, as shown in Fig. 11(c). The above facts indicate that the pinning effect of θ' precipitate becomes seriously weakened under the elevated temperature, which leads to the decrease of strength of 2519A aluminum alloy.

4 Conclusions

1) The dynamic mechanical properties of 2519A-T87 aluminum alloy exhibit strain rate susceptibility and temperature susceptibility. At the elevated temperature (250−350 °C), the θ' precipitate coarsens and mostly transforms into steady θ phase, which results in the rapidly decrease of flow stress.

2) There is a critical point on the dynamic true stress−strain curves. The original Johnson-Cook and

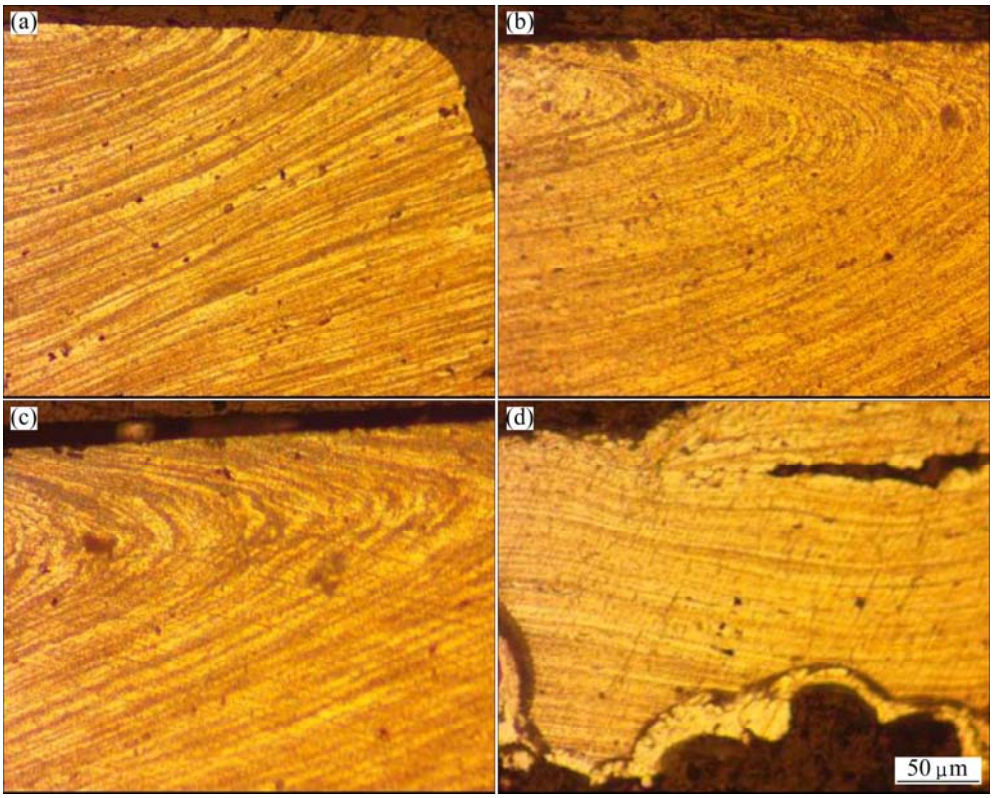

Fig. 10 Optical micrographs of aluminum alloy 2519A impacted at different strain rates (350 °C): (a) 1600 s^{-1}; (b) 2205 s^{-1}; (c) 3282 s^{-1}; (d) 5297 s^{-1}

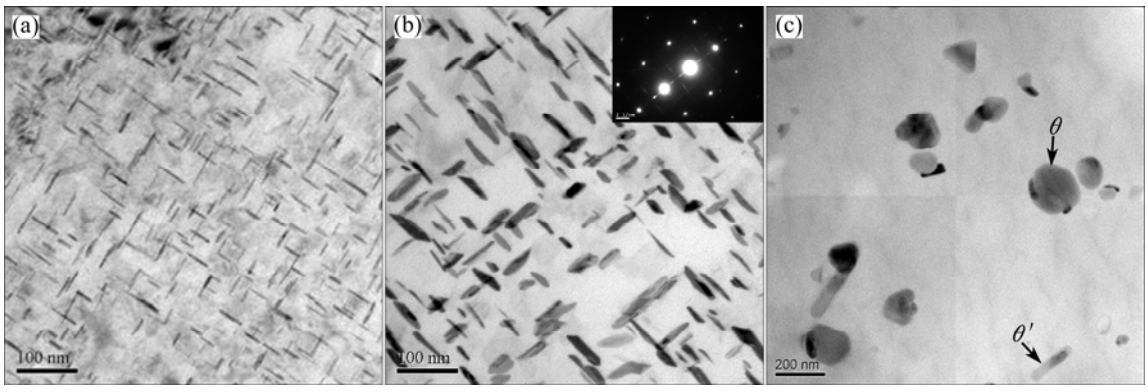

Fig. 11 TEM micrographs of 2519A aluminum alloy under different conditions: (a) Specimen before impact at room temperature; (b) Specimen before impact at 350 °C for holding 5 min; (c) Specimen after impact at 350 °C and 3282 s^{-1}

modified Johnson-Cook constitutive equations of 2519A aluminum alloy satisfy:

$$\sigma = (452.68 + 282.6\varepsilon^{0.42})(1 + 0.0142\ln\dot{\varepsilon}^{*})(1 - T^{*0.74})$$

$$\sigma = 452.68(1 + 2.54\varepsilon - 10.8\varepsilon^{2})(1 + 0.0142\ln\dot{\varepsilon}^{*})(1 - T^{*0.74})$$

3) The crack forms and mainly extends along ASB at normal temperature (20−150 °C). At elevated temperature (250−350 °C), a number of deformation structures are observed, and there is no ASB in the impacted specimen ($\dot{\varepsilon}$ <5300 s^{-1}). 2519A aluminum alloy mainly undergoes large sliding and plastic deformation under dynamic impact at elevated temperature.

References

[1] DANNEMANN K A, SIDNEY C, CHARLES E A, Jr. Comparison of mechanical and constitutive response for five aluminum alloys for armor applications [C]//16th US National Congress of Theoretical and Applied Mechanics. San Antonio, TX, USA: Southwest Research Institute, 2010: 1−2.

[2] ZHANG X M, LI H J, LI H Z, GAO H, GAO Z G, LIU Y, LIU B. Dynamic property evaluation of aluminum alloy 2519A by split Hopkinson pressure bar [J]. Transactions of Nonferrous Metals Society of China, 2008, 18(1): 1−5.

[3] ZHANG Xin-ming, GAO Zhi-guo, CHEN Ming-an, LI Hui-jie, LIU Ying, LIU Bo. Microstructure transformation of 2519A aluminium alloy impacted at high strain rates [J]. The Chinese Journal of Nonferrous Metals, 2008, 18(8): 1371−1376. (in Chinese)

[4] GAO Zhi-guo, ZHANG Xin-ming, CHEN Ming-an, ZHAO Yi-sheng, LI Hui-jie, LIU Bo. The effect of temperature on dynamic yield stress of 2519A aluminium alloy and its microstructure under high strain rates [J]. Rare Metal Materials and Engineering, 2009, 38(5): 881−886. (in Chinese)

[5] LI H Z, ZHANG X M, CHEN M G, LIU Y, GAO H. Hot deformation behavior of 2519 Al alloy during isothermal compression [J]. Materials Science Forum, 2007, 546: 749−754.

[6] LI H Z, LIANG X P, ZHANG X M, HUANG B Y, ZHANG C F. Microstructure evolution of 2519 aluminum alloy during hot deformation [J]. Transactions of Nonferrous Metals Society of China, 2010, 20(2): 189−194.

[7] LIN Q Q, PENG D S, ZHU Y Z. Establishment of constitutive relationship model for 2519 aluminum alloy based on BP artificial neural network [J]. Journal of Central South University of Technology, 2005, 12(4): 380−384.

[8] LIANG X P, LI H Z, HUANG L, HONG T, MA B, LIU Y. Microstructural evolution of 2519-T87 aluminum alloy obliquely impacted by projectile with velocity of 816 m/s [J]. Transactions of Nonferrous Metals Society of China, 2012, 22(6): 1270−1279.

[9] GAO H, ZHANG X M, LI H Z, LIU Y. Microsructure inhomogeneities in 2519A aluminum plate penetrated by an incendiary projectile [J]. Materials Science Forum, 2007, 546: 1049−1054.

[10] GAO Z G, ZHANG X M, CHEN M. Investigation on θ' precipitate thickening in 2519A-T87 aluminum alloy plate impacted [J]. Journal of Alloys and Compounds, 2009, 476(1−2): 1−3.

[11] GORDON R J, WILLIAN H C. Fracture characteristics of three metals subjected to various strains, strain rates, temperatures and pressures [J]. Engineering Fracture Mechanics, 1985, 21(1): 31−48.

[12] YU Tong-xi, QUI Xing-min. Impact dynamics [M]. Beijing: Tsinghua University Press, 2011: 49−52. (in Chinese)

[13] ZHAO Yi-sheng. ZHANG Xin-ming. Yield constitutive model of Al−5.8Cu alloy [J]. Material & Heat Treatment, 2012, 41(4): 55−57. (in Chinese)

[14] MILANI A S, DABBOUSSI W, NEMES J A, ABEYARATNE R C. An improved multi-objective identification of Johnson–Cook material parameters [J]. Materials Science and Engineering, 2008, 36(2): 294−302.

[15] DIPI S, SUNATRA M, BHADURI A K. A comparative study on Johnson-Cook, modified Zerill-Armstrong and Arrhenius-type constitutive models to predict elevated temperature flow behaviour in modified 9Cr−1Mo steel [J]. Computational Materials Science, 2009, 47(2): 568−576.

[16] WANG L L, YU T X, LI Y C. Impact dynamics [M]. Hefei: University of Science and Technology of China Press, 1992: 1−26. (in Chinese)

[17] LI X, ZHANG H B, RUAN X Y, LUO Z H, ZHANG Y. Analysis and modeling of flow stress of 40Cr steel [J]. Journal of Materials Engineering, 2004(11): 41−49.

2519A 铝合金的动态力学性能及本构关系

刘文辉，何圳涛，陈宇强，唐思文

湖南科技大学 机电工程学院，湘潭 411201

摘　要：为研究应变速率及温度对 2519A 铝合金流变应力的影响，对 2519A 铝合金进行动态力学性能测试及准静态拉伸实验，结合光学显微镜及透射显微电镜分析应变速率及温度对微观组织演化的影响。研究结果表明：2519A 铝合金具有应变速率效应及温度敏感性。采用变量分离与非线性拟合方法对准静态及霍普金森压杆（SHPB）实验数据进行拟合，得到 2519A 铝合金的 Johnson-Cook 本构模型参数，曲线拟合与实验结果吻合较好，为力学性能的研究及抗弹性能有限元分析提供了参考。

关键词：2519A 铝合金；动态力学性能；Johnson-Cook 模型；微观组织

(Edited by Yun-bin HE)